Magnetic phase transition in the metal-rich rare-earth carbide halides Gd_2XC (X = Br,I)

R. Reisser,* R.K. Kremer, and A. Simon
Max-Planck-Institut für Festkörperforschung, Postfach 800665, D-70506 Stuttgart, Germany
(Received 6 March 1995; revised manuscript received 13 April 1995)

The critical behavior of the ferromagnetic-paramagnetic phase transition of metal-rich rare-earth carbide halides Gd_2BrC and Gd_2IC is investigated. These compounds exhibit a layered structure of Gd–C–Gd slabs which are sandwiched between layers of halogen atoms (Br,I). The critical exponents β, γ', γ, and δ are determined by several methods: modified Arrott plots, Kouvel-Fisher plots, scaling plots, and $\ln J$ vs $\ln(\mu_0 H)$ plots. The asymptotic critical exponents β and γ as well as the critical amplitudes J_0 and h_0/J_0 were determined from both the Kouvel-Fisher and the correction to scaling analysis. The derived critical exponents are identical for all methods and in good agreement with the predictions of the three-dimensional Heisenberg model whereas the reduced critical amplitudes $J_0/J_S(0)$, $\mu h_0/k_B T_c$, and $D J_0^{\delta}/h_0$ cannot be related to a particular model. The temperature dependence of the Kouvel-Fisher exponent $\gamma(T)$ is discussed with respect to chemical disorder.

I. INTRODUCTION

Metal-rich halides of the rare-earth elements represent a new class of compounds which exhibit a number of interesting properties.[1–6] In general the metal-rich halides contain building blocks (e.g., chains or layers of metal atoms) which are embedded and charged balanced by surrounding halogen atoms. These metal-rich units generally accomodate interstitial atoms (e.g., H,C) or even transition-metal atoms (e.g., Fe,Co). Earlier studies of their physical properties have detected ferromagnetism in some of these compounds with transition temperatures ranging up to almost room temperature.[2,6] The occurrence of a ferromagnetic ordering in these compounds allows the study of the critical behavior at the phase transition from the ferromagnetic (ferrimagnetic) state to the paramagnetic state. Such an analysis is performed to test whether the observed phase transition is a real second-order transition and to gain a better insight into main exchange mechanisms.

Recently, we have analyzed in detail the magnetic phase transition of the metal-rich halides Gd_2BrFe_2, Gd_2IFe_2, and Gd_2ICo_2.[7] These compounds crystallize in a layered structure wherein the intermetallic slabs formed by Gd-(Fe,Co)-Gd are separated by a single layer of halogen (Br,I) atoms (Fig. 1). The critical exponents experimentally determined for these compounds are in best agreement with those derived for the three-dimensional (3D) XY model. This result implies that the magnetic moments of both Gd and the transition-metal atom (Fe,Co) are confined to lie within the intermetallic slabs. We attributed the appearance of this strong planar anisotropy to pronounced anisotropic exchange interactions induced by the $3d$ electrons of the transition-metal atoms.

Another series of metal-rich rare-earth halide compounds which order ferromagnetic are the metal-rich carbide halides Gd_2BrC and Gd_2IC.[2] In these compounds the $3d$ transition-metal atoms are substituted by carbon atoms which are octahedrally surrounded by Gd atoms. Such Gd_6C octahedra are connected via common edges to form layers which are again sandwiched by layers of halogen atoms (Br,I) (Fig. 1).

To check if the aforementioned strong planar

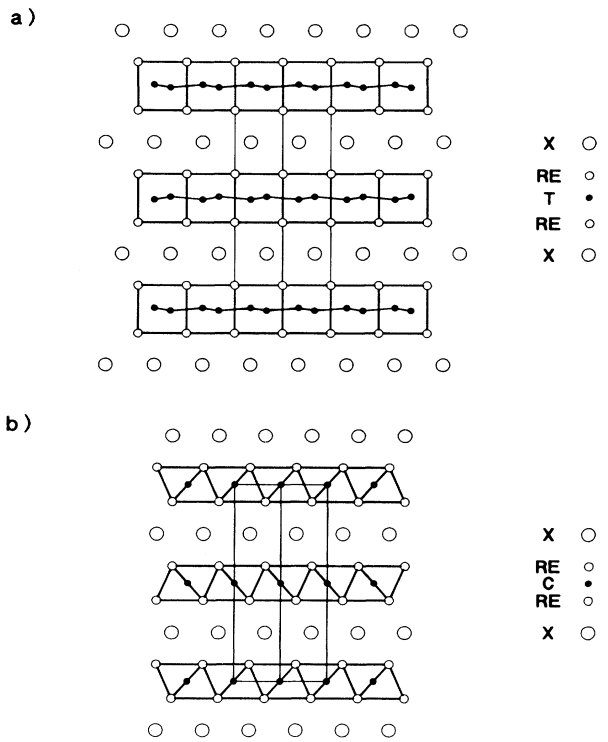

FIG. 1. A projection of the structures of RE_2XT_2 (a) (Refs. 6 and 7) and RE_2XC (b) (Ref. 2) along the [110] direction. Abbreviations are RE: rare earth (Gd); T: transition metal (Fe,Co); X: halogen (Br,I); and C: carbon atoms, respectively.

anisotropy can be modified by a variation of the type of intersticials we carried out a detailed analysis on the critical behavior of the carbide halides Gd_2XC (X = Br,I).

II. THEORY

An analysis of the magnetic phase transition is based on the determination of the critical parameters to test the predictions of different models. In the critical regime ($t \to 0, t = T/T_c - 1$) the critical exponents β, γ', γ, and δ describe the temperature dependence of the spontaneous polarization J_S, the inverse zero field susceptibility χ' for $T < T_c$ and χ for $T > T_c$, respectively, and the field dependence of the polarization $J(\mu_0 H, T = T_c)$ for the critical isotherm as follows:

$$J_S = J_0 (-t)^{\beta} \ (t \to 0, \ t \leq 0, \ \mu_0 H = 0) \ , \tag{1}$$

$$\chi^{-1} \sim (-t)^{\gamma'} \ (t \to 0, \ t \leq 0, \ \mu_0 H = 0) \ , \tag{2}$$

$$\chi^{-1} = \left(\frac{h_0}{J_0}\right) t^{\gamma} \ (t \to 0, \ t \geq 0, \ \mu_0 H = 0) \ , \tag{3}$$

and

$$(\mu_0 H) = D \, J^{\delta} \ (t = 0) \ . \tag{4}$$

These critical exponents are universal quantities in the corresponding universality class and, therefore, they depend only on the spatial and the order parameter dimensionalities d and n if the exchange energy declines stronger than $1/r^{d+2}$. Such a prerequisite implies that the exchange coupling of the magnetic moment is of short-range order. Nearest-neighbor interactions are assumed in the 3D Ising model ($n = 1$) and the 3D Heisenberg model ($n = 3$) of which the critical exponents are listed in Tables I and II. Moreover, only two exponents are independent since the others are related to each other via the following scaling relation:

$$\gamma' = \gamma = \beta (\delta - 1) \ . \tag{5}$$

The prefactors J_0, h_0/J_0, and D in Eqs. (1), (3), and (4) are denoted as critical amplitudes.[8,9] To obtain also universal quantities, the reduced values of critical amplitudes $\mu \, h_0/k_B \, T_c$ and $D \, J_0^{\delta}/h_0$ and the ratio $J_0/J_S(0)$ are determined (Tables I and II). From a comparison of the theoretical predictions with experimental results, conclusions can be made concerning the dominant exchange and spin arrangement in the material investigated.

The critical exponents can be determined from temperature- and field-dependent measurements of the magnetic polarization $J(\mu_0 H, T)$ by several methods: modified Arrott plots, Kouvel-Fisher plots, scaling plots, and $\ln J$ vs $\ln(\mu_0 H)$ plots. In addition to the method of Kouvel-Fisher (KF) which is used to extract the critical exponents β (γ), the critical temperature T_c and the width of the critical regime, we applied the correction-to-scaling (CTS) analysis. This method yields a more detailed information concerning the asymptotic critical behavior.[10–15] As asymptotic critical exponents we denote exponents which are obtained from an analysis in the asymptotic critical regime (ACR: $t \leq 10^{-2}$). This analysis is based on the following expressions for the spontaneous polarization $J_S(T)$ and the zero field susceptibility $\chi^{-1}(T)$:

$$J_S(T) = J_0 (-t)^{\beta} [1 + a_J^- (-t)^{\Delta}] \ (t < 0, \ \mu_0 H = 0) \tag{6}$$

and

$$\chi^{-1}(T) = (h_0/J_0) t^{\gamma} [1 + a_\chi^+ (t)^{\Delta}] \ (t > 0, \mu_0 H = 0). \tag{7}$$

In addition to the power laws [Eqs. (1) and (3)], these expressions [Eqs. (6) and (7)] contain the so-called CTS term a_J^- (a_χ^+) arising from the irrelevant scaling fields as predicted by the renormalization-group (RG) calculations.[15–17] In these terms the plus or minus sign denotes whether the fit parameters T_c and a_J^- (a_χ^+) are obtained from data for $t < 0$ or $t > 0$. The exponent Δ was kept constant at its theoretical prediction for the 3D Heisenberg model $\Delta = 0.55$. It should be noted that fitting the power laws [Eqs. (1) and (3)] to the corresponding data yields *effective* critical exponents even if a critical regime $t < 10^{-2}$ is considered, since the exponent value depends on the temperature range chosen for the fit. To assure that the asymptotic critical exponents are obtained, the CTS analysis is applied according to Ref. 15.

TABLE I. Critical exponents as derived from both different experimental methods and theoretical models. Abbreviations are MA: modified Arrott plot; KF: Kouvel-Fisher plot; SP: scaling plot; LNP: $\ln J$ vs $\ln(\mu_0 H)$ plot; SL: scaling law Eq. (5); ($d = 3$, $n = 3$): 3D Heisenberg model; ($d = 3$, $n = 1$): 3D Ising model.

	MA			KF		SP			LNP	SL
	β	γ'	γ	β	γ	β	γ'	γ	δ	δ
Gd_2BrC	0.365(8)	1.387(8)	1.387(8)	0.379(5)	1.380(6)	0.380(2)	1.382(3)	1.380(4)	4.80(25)	4.73(13)
Gd_2IC	0.380(8)	1.380(8)	1.380(8)	0.380(5)	1.370(7)	0.370(4)	1.385(5)	1.390(6)	4.68(25)	4.69(15)
($d = 3$, $n = 3$) (Refs. 8, 45)	0.365(3)		1.386(4)						4.80(4)	
($d = 3$, $n = 1$) (Refs. 8, 45)	0.325(2)		1.241(2)						4.82(2)	

TABLE II. Values experimentally determined for the magnetic saturation and the critical amplitudes as well as a comparison of the reduced critical amplitudes with the theoretical predictions of different models. Abbreviations are $J_S(T = 5\,\mathrm{K})$: the saturation polarization at $T = 5\,\mathrm{K}$; μ: the magnetic moment per formula unit; ($d = 3$, $n = 3$): 3D Heisenberg model; ($d = 3$, $n = 1$): 3D Ising model.

	$J_S(T = 5\,\mathrm{K})$ (T)	μ (μ_B)	J_0 (T)	h_0/J_0	D ($\mathrm{T}^{1-\delta}$)	J_0/J_S	$\frac{\mu h_0}{k_B T_c}$	$\frac{D J_0^\delta}{h_0}$
Gd_2BrC	1.56(2)	11.9(2)	1.30(10)	34(4)	17(1)	0.83(8)	3.34(25)	1.38(30)
Gd_2IC	1.33(2)	10.4(2)	1.02(10)	131(10)	65(4)	0.78(8)	5.30(25)	0.53(20)
($d = 3$, $n = 3$)						1.37(7)	1.58	1.33(1)
(Refs. 8, 45)								
($d = 3$, $n = 1$)						1.486(1)	1.52	1.81(1)
(Refs. 8, 45)								

III. EXPERIMENTAL DETAILS

The sample preparation and the structural analysis as well as a first investigation on the magnetic properties is given in Ref. 2. Here, we emphasize only details concerning the magnetic measurements. The samples were sealed in quartz capillaries to avoid any contact with moisture and oxygen. Since the magnetic moment of these capillaries is three orders of magnitude lower than the smallest magnetic moment measured, it could be neclected. The measurements were carried out with a superconducting quantum interference device magnetometer (type: MPMS, Quantum Design) in external fields $\mu_0 H_{\mathrm{ext}}$ up to 1 T and in the temperature range $5\,\mathrm{K} \leq T \leq 280\,\mathrm{K}$. As temperature steps for the measurement of the isotherms we used $\Delta T = 0.5, 1, 2, 5, 10\,\mathrm{K}$. To assure that the temperature accuracy within an isotherm is better than the smallest temperature step size, we did not chose a step smaller than 0.5 K. The internal field $\mu_0 H$ was calculated by subtracting the demagnetizing field $N J$ from the external field $\mu_0 H_{\mathrm{ext}}$.

IV. DATA ANALYSIS AND RESULTS

The critical exponent values and the critical temperature extracted by several methods are summarized in Tables I and III, respectively. In Table IV we present the fit parameters obtained by both the KF and the CTS analysis. As fit range we denote the temperature range for which the corresponding fit is characterized by the smallest standard deviation. The magnetic saturation at $T = 5\,\mathrm{K}$, the critical amplitudes, as well as the reduced critical amplitudes are listed in Table II. The uncertainty limits given in Tables I–IV show the range in which the deviation is constant within the error bars.

At first the temperature dependence of the polarization J was measured at low fields ($\mu_0 H_{\mathrm{ext}} < 2$ mT) for a rough estimate of the critical temperature T_c (Table III). In the so-called kinkpoint measurement, the polarization J nearly drops to zero after a sharp kink at the critical temperature T_c (Fig. 2). Furthermore the kinkpoint measurement can be used to check whether or not the material investigated is magnetically single phase. If an additional magnetic phase with a higher critical temperature T_c^* as the one of the main phase exists, the polarization J does not vanish well above T_c. Considering the temperature dependence of the polarization J in Fig. 2, we conclude that Gd_2BrC and Gd_2IC are magnetically single phase.

As a first method to extract the critical parameters β, γ', γ, and T_c we used modified Arrott plots in which the measured polarization curves are represented in the form $J^{1/\beta}$ vs $(\mu_0 H/J)^{1/\gamma}$. The exponents β and γ are chosen in such a way that the isotherms close to the critical one show an almost linear variation. The critical isotherm ($T = T_c$) is the one which passes through the

TABLE III. Values for the critical temperature T_c as derived from different methods. Abbreviations are KP: kinkpoint; MA: modified Arrott plot; KF: Kouvel-Fisher plot; SP: scaling plot; LNP: $\ln J$ vs $\ln(\mu_0 H)$ plot.

	KP T_c(K)	MA T_c(K)	KF T_c^-(K)	KF T_c^+(K)	LNP T_c(K)	SP T_c(K)
Gd_2BrC	108(4)	105.5(5)	105.6(2)	105.9(2)	105.5(5)	105.9(2)
Gd_2IC	178(4)	176.7(5)	176.2(2)	176.1(3)	176.0(5)	176.1(2)
Gd_2BrFe_2	270(3)	269.5(5)	269.7(3)	269.9(2)	269.5(5)	269.9(2)
(Ref. 7)						
Gd_2IFe_2	280(3)	279.5(5)	279.5(2)	279.4(2)	279.5(5)	279.4(2)
(Ref. 7)						

TABLE IV. Fit parameters for the spontaneous polarization $J_S(T)$ and the inverse zero field susceptibility $\chi^{-1}(T)$. Abbreviations are KF: Kouvel-Fisher; CTS: correction to scaling.

	Analysis	Fit range t	T_c^- (K)	β	J_0 (T)	a_J^-	Fit range t	T_c^+ (K)	γ	h_0/J_0	a_J^-
Gd_2BrC	KF	3.68×10^{-2}	105.9(4)	0.372(5)	1.30(10)		3.90×10^{-2}	105.9(1)	1.386(6)	44(2)	
	CTS	2.72×10^{-2}	105.88(2)	0.365(5)	1.30(10)	−3.7(8)	2.03×10^{-2}	105.85(1)	1.392(8)	34(4)	−2.3(2)
Gd_2IC	KF	1.82×10^{-2}	176.2(4)	0.373(8)	0.98(10)		3.30×10^{-2}	176.0(2)	1.375(5)	74(2)	
	CTS	1.80×10^{-2}	176.17(1)	0.375(8)	1.02(10)	−5.6(3)	1.60×10^{-2}	176.18(2)	1.370(8)	131(10)	7.5(8)

origin (Fig. 3) (Tables I and III). Since we use different values for γ for the isotherms below and above T_c, we can determine γ' and γ independently. In Fig. 3 the so-called low field data show a deviation from linearity. Such a behavior was found in a series of earlier investigations for numerous materials.[7,8,18–27] To get rid of these anomalies an extrapolation of the high field data range ($\mu_0 H \geq 0.1$ T) which is characterized by a linear variation is performed.[7,8,21–26] The spontaneous polarization J_S and the inverse zero field susceptibility χ^{-1} are obtained from the interceptions with the $J^{1/\beta}$ axis and the $(\mu_0 H/J)^{1/\gamma}$ axis, respectively. Furthermore, we fitted a cubic spline to both the spontaneous polarization $J_S(T)$ and the inverse zero field susceptibility $\chi^{-1}(T)$. This spline was used to calculate the Kouvel-Fisher quantities $J_S^{-1}(dJ_S^{-1}/dT)$ and $\chi^{-1}(d\chi^{-1}/dT)$ numerically. Plotting these quantities as function of temperature T yields straight lines in the vicinity of the critical temperature ($T \to T_c$) and the inverse slope corresponds to β and γ, respectively[7,8,10,18–28] (Tables I and III).

A further possibility for the evaluation of the critical exponents β, γ', γ, and the critical temperature T_c is given by the scaling analysis. If the scaling hypothesis is valid, there exists a reduced equation of state in the form

$$\frac{J}{|t|^\beta} = f_\pm \frac{(\mu_0 H)}{|t|^{\beta+\gamma}}, \tag{8}$$

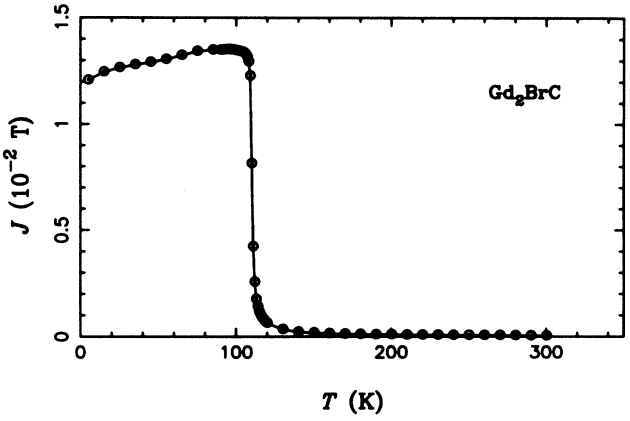

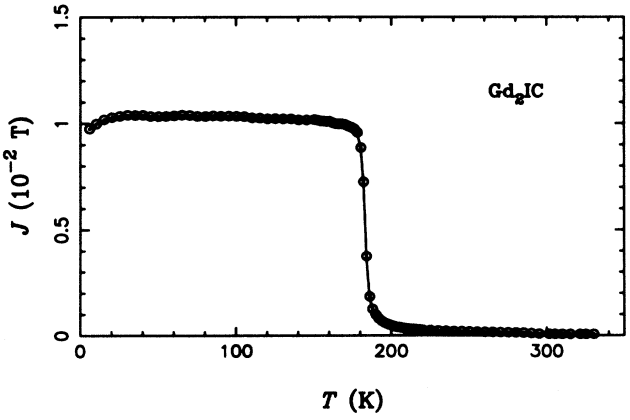

FIG. 2. Kinkpoint measurement for both Gd_2BrC and Gd_2IC.

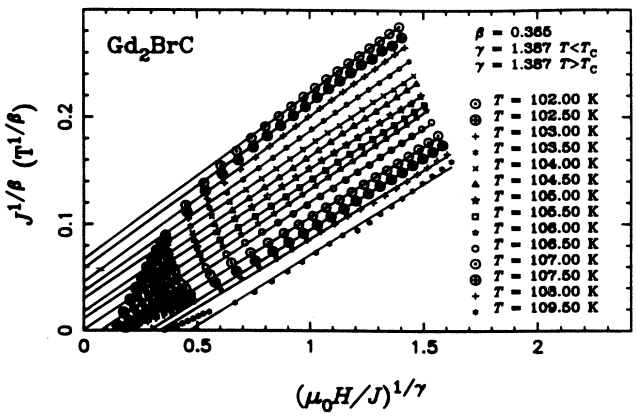

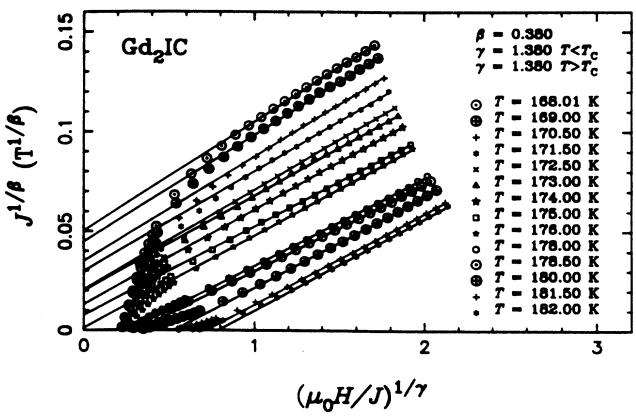

FIG. 3. Modified Arrott plots for a selection of isotherms in the critical regime.

where f is a scaling function and the plus or minus sign denotes the ferromagnetic and paramagnetic region, respectively. In the scaling plots the data are plotted in the form $\ln(J/|t|^{\beta})$ vs $\ln(\mu_0 H/|t|^{\beta+\gamma})$ whereby a data collapse on two branches is observed if the correct critical parameters β, γ', γ, and T_c are chosen. Figure 4 shows such a scaling plot with optimized parameters for Gd_2BrC. The upper branch represents the ferromagnetic range ($T < T_c$) and the lower branch the paramagnetic region ($T > T_c$). Once again, we test the validity $\gamma' = \gamma$ by using different values of γ for the data below and above T_c (Fig. 4) (Tables I and III). It should be noted that an optimum data collapsing is only observed by using the high field data ($\mu_0 H \geq 0.1\,\mathrm{T}$).[8,22–26] Earlier investigations[22,29] have shown that taking into account data from outside the critical regime a good scaling behavior could also be observed. Since for some data sets it is not obvious when the deterioration from the optimum data collapsing occurs, we additionally performed the KF and CTS analysis where the critical regime can be determined more accurately.

The exponent δ which describes the field dependence of the critical isotherm ($T = T_c$) can be easily determined when plotting the quantities $\ln J$ vs $\ln(\mu_0 H)$. In this graph the critical isotherm is characterized by an almost linear variation. For materials with a negligible anisotropy the isotherms for $T < T_c$ have a concave and for $T > T_c$ a convex curvature, whereas for materials with a non-negligible anistropy all isotherms show a convex curvature (Fig. 5). The exponent δ is obtained from the inverse slope of the critical isotherm (Tables I and III). Again, we find reasonable values for δ only when performing a linear regression on the so-called high field data ($\mu_0 H \geq 0.1\,\mathrm{T}$).[7,21–23,25,26,30,31] Moreover, this plot allows the determination of the critical amplitude D from the interception of the critical isotherm with the $\ln J$ axis numerically[7,9,26,31] (Table II).

In addition to the determination of critical parameters β (γ) and T_c, the application of the KF analysis yields the critical amplitudes J_0 and h_0/J_0, respectively. This analysis is based on fitting the corresponding power law [Eqs. (1) or (3)] to the data of $J_S(T)$ and $\chi^{-1}(T)$. To obtain optimized least-squares fits we varied the exponent β (γ) and the width of the critical regime while the critical temperature T_c was kept constant for a series of fits. The fit parameters obtained for the best fit which is characterized by the smallest standard deviation are listed in Tables II and IV, respectively.

As described in Sec. I, the CTS analysis can be used as a further tool to extract the critical parameters β (γ), T_c, J_0 (h_0/J_0), and the width of the critical regime.[10,15] In contrast to the KF method, the CTS analysis is based on fitting least-squares fits according to Eqs. (6) and (7) to the data of $J_S(T)$ and $\chi^{-1}(T)$ (Fig. 6). Applying this procedure, we kept the exponent constant for a series of least-squares fits (characterized by the same ACR) whereas J_0 (h_0/J_0), T_c^- (T_c^+), and a_J^- (a_χ^+) were left as adjustable parameters. For the exponent Δ we used the value predicted for the 3D Heisenberg model, $\Delta = 0.55$. Again, the fit parameters for which the best fit was obtained are presented in Tables II and IV. The saturation polarization $J_S(0)$ which is necessary to calculate the reduced critical amplitude $J_0/J_S(0)$ was ascertained from measuring the magnetic moment at $T = 5\,\mathrm{K}$ and in external fields up to $\mu_0 H_{\mathrm{ext}} = 5.5\,\mathrm{T}$.

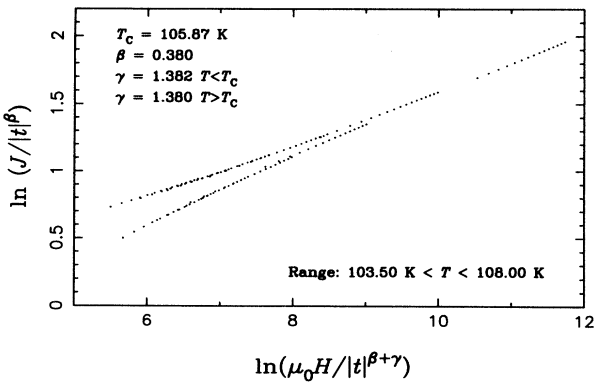

FIG. 4. Scaling plot for Gd_2BrC.

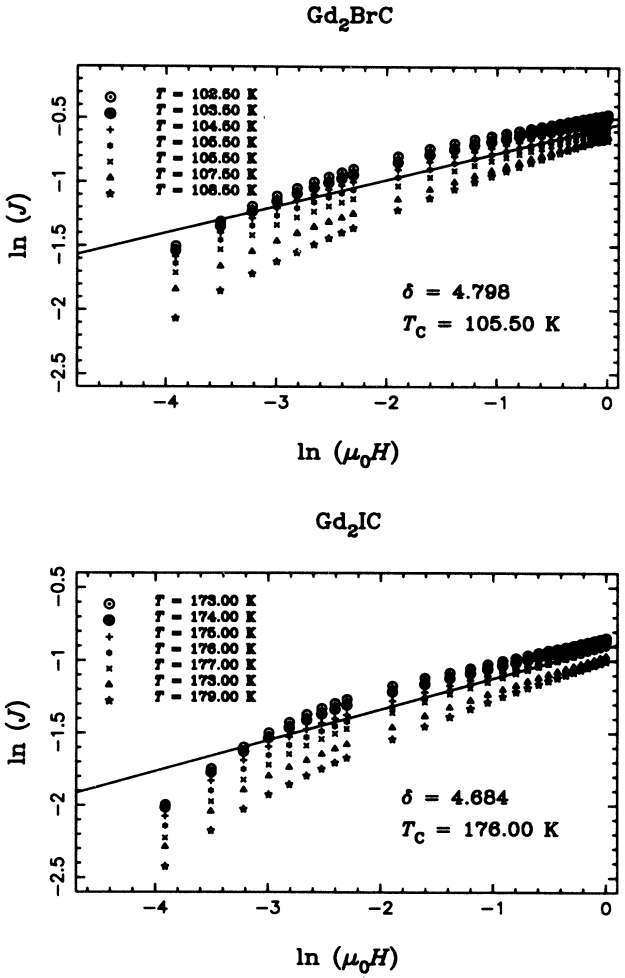

FIG. 5. Plots of $\ln J$ vs $\ln(\mu_0 H)$ at a few temperatures around the critical temperature T_c. The straight line represents the best least-squares fit to the so-called high field data, i.e., $\mu_0 H \geq 0.1\,\mathrm{T}$.

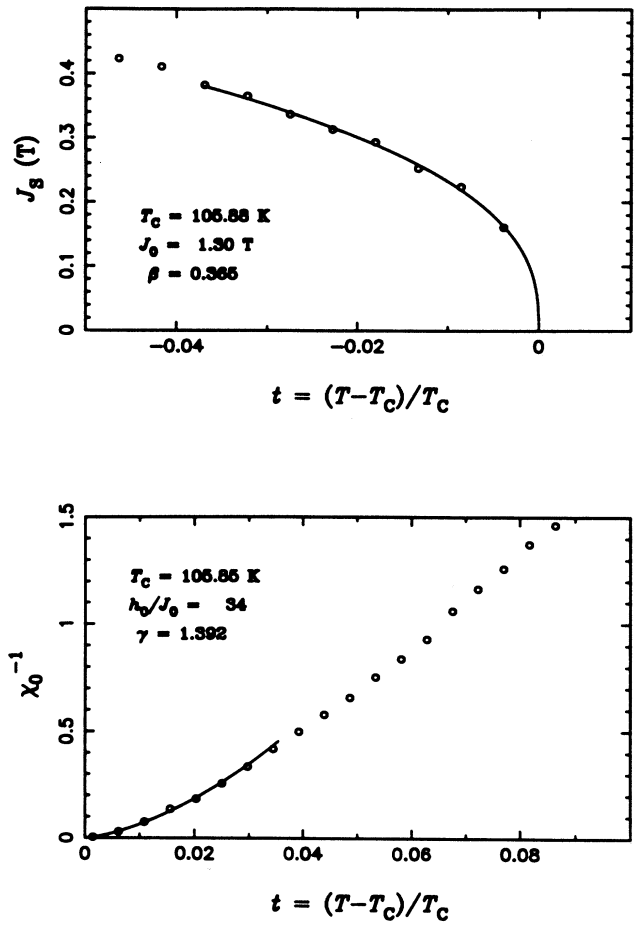

FIG. 6. Temperature dependence of both the spontaneous polarization J_S and the inverse zero field susceptibility χ^{-1} for Gd_2BrC. The full line represents the CTS least-squares fit according to Eqs. (6) and (7).

V. DISCUSSION

The metal-rich carbide halides Gd_2XC and Gd_2XC (X = Br,I) exhibit ferromagnetism like the recently investigated metal-rich halides Gd_2XT_2 (T = Fe,Co). The crystal structure of both series of compounds is similar: a sandwich structure formed by layers of halogen atoms (Br,I) and layers of Gd and Fe (Co) or C atoms is the common feature (Fig. 1). In both cases metal atom layers are sandwiched between layers of halogen atoms. However, while the metal-rich carbide halides contain trigonal antiprisms of Gd_6C which are connected via common edges to form closed packed metal atom bilayers, in the structures of Gd_2XT_2 trigonal prisms are condensed into intermetallic slabs of Gd-T-Gd. In view of the similarities but also the distinct differences, we performed a detailed analysis of the magnetic phase transition of Gd_2BrC and Gd_2IC in order to test whether the substitution of the transition metals Fe and Co, respectively, by C atoms and/or the different structure within the magnetic layers (composed of atoms which have a magnetic moment) has a crucial influence on the magnetic critical properties.

The critical temperature T_c for Gd_2BrC and Gd_2BrC is distinctly lower than room temperature (Table III). This result is in contrast to the compounds Gd_2BrFe_2 and Gd_2BrFe_2 for which critical temperatures close to room temperature were found (Table III). However, a difference between the critical temperatures of the metal-rich carbide halides and the metal-rich halides may be expected because a substitution of the transition-metal atoms (Fe,Co) by C atoms together with a change of the structure within the magnetic layers must have an influence on the strength of the exchange interactions and therefore on the critical temperature T_c. Moreover, it should be mentioned that both types of metal-rich halides show a higher critical temperature T_c when containing iodine instead of bromine, and this feature is more pronounced for the carbide halides.

The critical exponents extracted for Gd_2BrC and Gd_2IC by different methods are in best agreement with the values derived for the 3D Heisenberg model. In addition, all exponent values fulfill the scaling relation Eq. (5). We therefore conclude that the critical behavior of the metal-rich carbide halides Gd_2BrC and Gd_2IC can be described within the framework of the 3D Heisenberg model. A prerequisite of this model is that the magnetic exchange interactions are of short-range order, and both the order parameter dimensionality n and the space dimensionality d are equal to 3.

This result is in strong contrast to the one elaborated for the compounds Gd_2BrFe_2 and Gd_2IFe_2 for which the critical exponents are in best agreement with predictions derived for the 3D XY model.[7] We ascribed such a behavior to the occurrence of a strong planar anisotropic exchange interaction induced by the 3d transition metals Fe or Co. We therefore suppose that this anisotropic exchange interaction should be weakened or even disappearing in materials with a similar structure (Sec. I, Fig. 1) when substituting the 3d transition-metal atoms (Fe,Co) by nonmagnetic atoms (e.g., C). The present study confirms this assumption. Furthermore, we assume that a separation of the magnetic layers is not the only requirement which is necessary for the occurrence of a strong planar anisotropy. Indeed, it must be the distance between the magnetic layers as well as the arrangement of the 3d transition-metal atoms and the rare-earth metal atoms within the intermetallic slabs which is responsible for the observed 3D XY behavior in the compounds Gd_2BrFe_2 and Gd_2IFe_2. In contrast, if the magnetic slabs are only formed by Gd and C atoms as shown in Fig. 1, the 3D Heisenberg behavior which describes the critical behavior for numerous materials is found.[8,10,21–23,25,26,30,32] It should be noted that the critical behavior of the compounds Gd_2BrC and Gd_2IC differs from the one observed for pure Gd metal. For Gd single crystals the critical exponent β is more Heisenberg-like with a tendency towards the mean field value whereas the exponent γ is Ising-like.[33–35]

In addition to the critical exponents we determined the temperature-dependent Kouvel-Fisher exponent

$$\gamma(T) = (T - T_c)\,\chi(T)\,\frac{d\chi^{-1}(T)}{dT}, \qquad (9)$$

which describes the temperature dependence of $\chi^{-1}(T)$ in the temperature range between the ACR ($t \to 0$) and the Curie-Weiss range ($t \to \infty$). For isotropic homogeneous ferromagnets this exponent starts at the asymptotic critical value and decreases monotonically to the mean field value $\gamma = 1$ with rising temperature. A series of investigations[7,25,30,31] has shown that *chemical* disorder already causes the typical nonmonotonic temperature dependence with a maximum at reduced temperatures $t = 0.1 \ldots 0.5$ for $\gamma(T)$ as predicted by the correlated molecular field theory[36,37] and supported by Monte Carlo computer simulations.[36,38,39] In Fig. 7 we present the Kouvel-Fisher exponent $\gamma(T)$ for Gd_2BrC and Gd_2IC. This exponent shows for both metal-rich carbide halides the typical monotonic behavior as expected for homogeneous ferromagnets. Therefore, this result can be taken as strong evidence for the high *chemical* and *structural* order of these compounds.

The existence of a magnetic anisotropy in these compounds is pointed out by the modified Arrott plots (Fig. 3). In these plots the isotherms seem to coincide in a point shifted to the right from the origin on the $(\mu_0 H/J)^{1/\gamma}$ axis. Such a behavior has previously been detected for materials which are characterized by a magnetic anisotropy.[26] The size of this shift is a measure for the magnetic anisotropy,[26,40,41] either crystal anisotropy or random magnetic anisotropy. A further evidence for the occurrence of an anisotropy in these compounds is given by the $\ln J$ vs $\ln(\mu_0 H)$ plot (Fig. 5; cf. Sec. III). In this graph all isotherms show a convex curvature as found many times for materials with magnetic anisotropy.[7,25,26,30,31,42,43] Due to the perfect structure of the compounds investigated, we assume some macroscopic magnetic anisotropy arising from the layered structure and the arrangement of the atoms within the magnetic layers. However, since we have investigated isotropic powder samples (characterized by a random distribution of both the easy and hard directions) it is not possible to determine the easy and hard direction of these compounds.

As further methods for the determination of the width of the critical regime and the critical parameters T_c, β, γ, J_0, and J_0/J_S, we applied both the KF and the CTS analysis as described in Sec. III. The critical amplitude J_0 yields the same result when determined by the two different methods [Eqs. (1) and (6)] whereas large deviations are observed for the critical amplitude h_0/J_0. This difference is probably caused by the different width of the critical regime used for fitting Eqs. (3) and (7) to the data. However, we increased the width of the critical regime until the standard deviation of the corresponding fit deteriorates.

For a more detailed comparison of these different methods we focus our analysis on the fit parameters and the so-called "percentage deviation plots" as discussed in Ref. 15. There the KF as well as the CTS methods were applied to extract the critical parameters for polycrystalline Ni. This study yielded negative (positive) values for the CTS term a_J^- (a_χ^+). For Gd_2BrC a change of sign for the CTS term a_χ^+ is detected. It should be noted that for Gd_2BrC a positive value for this term (a_χ^+) could not be observed when varying both the width of the critical regime and the exponent γ or the critical temperature T_c. A possible reason for this result is based on the scattering of $\chi^{-1}(T)$ data in the critical regime which originates from a wavy course of some isotherms measured in the critical regime (cf. modified Arrott plots, Sec. III). We attribute a change of the curvature of these isotherms to experimental shortcomings of our magnetometer observed several times before independent of the particular material investigated. An evaluation of the quality of these two methods can be made when using the percentage deviation plots presented in Fig. 8 for Gd_2BrC. The deviation of the data of the spontaneous polarization $J_S(T)$ shows no obvious difference between the data obtained by the KF and the CTS analyses. In contrast, the percentage deviation plot for $\chi^{-1}(T)$ shows smaller deviations for the data obtained from the CTS analysis, especially for $t \to 0$. Such a behavior is expected from a

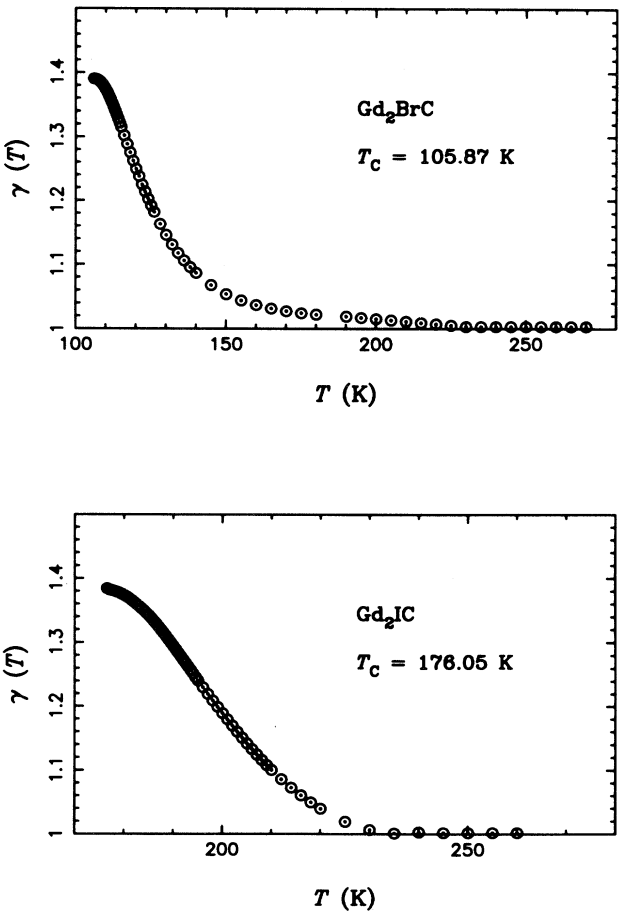

FIG. 7. The temperature dependence of the Kouvel-Fisher exponent $\gamma(T)$ for both Gd_2BrC and Gd_2IC.

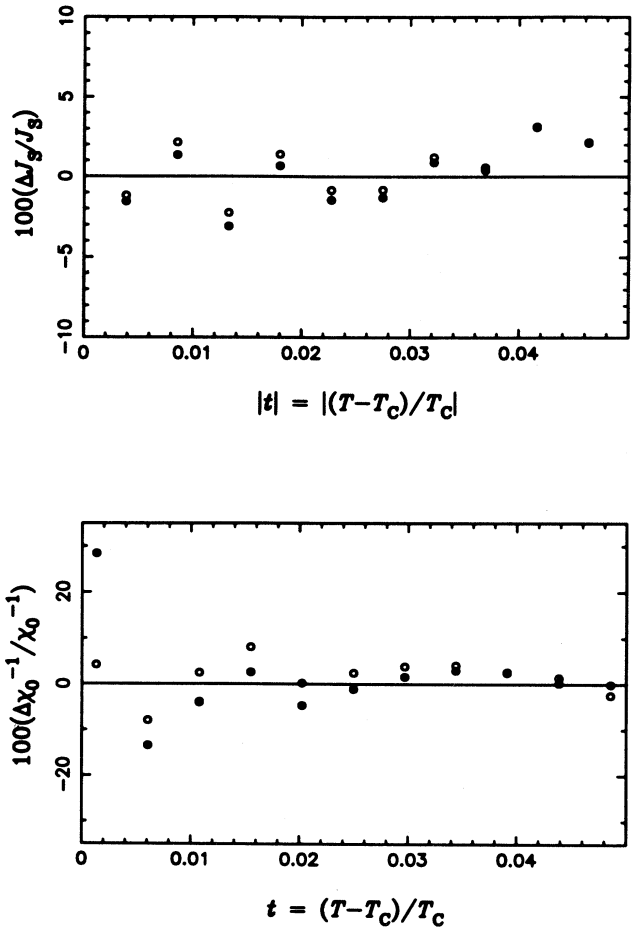

FIG. 8. Percentage deviation for both the spontaneous polarization J_S and the inverse zero field susceptibility χ^{-1} for Gd_2BrC. The closed circles denote the data obtained from the KF fit whereas the open circles denote the data obtained from the CTS fit.

more elaborate theory for the CTS analysis in order to determine the asymptotic critical parameters with better accuracy[15] (Sec. I). Comparing our results, we find that for the spontaneous polarization J_S both methods reveal no difference. If the critical regime (in our experiments estimated by KF plots, scaling plots, and the KF and CTS analysis) does not coincide with the asymptotic critical regime, the CTS analysis has no advantage over the KF analysis and consequently no improvement employing the CTS analysis concerning the percentage deviation may be expected.[15] However, we have shown that both the KF and the CTS analysis yield critical parameters for the compounds Gd_2BrC and Gd_2IC which are in accordance with the values extracted by other methods.

In Table II we present the critical amplitudes and the reduced critical amplitudes together with their theoretical predictions for both 3D Heisenberg and 3D Ising model. The values cannot be correlated to a particular model except for the amplitude ratio $D J_0^{\delta}/h_0$ of Gd_2BrC which agrees rather well with the 3D Heisenberg value. It has been shown that the determination of the critical amplitudes is much more sensitive to the data than the one of the critical exponents.[7,9,15,26,31,35,44] On the other hand, the methods used to extract the critical amplitudes yielded critical exponents (β, γ) and a critical temperature T_c which are in best agreement with the results obtained by the other methods. However, we think that the derived results for the reduced critical amplitudes are meaningful, and therefore they deserve some discussion. Surprisingly, the critical amplitude J_0/J_S is only about 60% of the 3D Heisenberg value for both compounds. This finding may indicate that only 60% of the magnetic moments in these compounds participate in the FM-PM phase transition.[15] A reason for the strong deviation of the reduced critical amplitudes J_0/J_S and $\mu h_0/k_B T_c$ for Gd_2BrC and Gd_2IC as well as $D J_0^{\delta}/H_0$ for Gd_2IC is not obvious. Impurities can be ruled out [see Kouvel-Fisher exponent $\gamma(T)$]. Perhaps the result is a trivial consequence of the polycrystalline nature of the sample. In this case it is conceivable that the irregular orientations of the grains preclude full alignment of the moments. However, if only 60% of the magnetic moments seem to actually participate in the magnetic phase transition, the critical amplitudes J_0 and h_0/J_0 are also affected and their reduced counterparts J_0/J_S and $\mu h_0/k_B T_c$ are expected to differ from the reduced critical amplitudes predicted by the 3D Heisenberg model.

To summarize, we have shown that the magnetic phase transition in the metal-rich carbide halides Gd_2BrC and Gd_2IC which are characterized by layered structure (consisting of layers of halogen and Gd-C atoms) can be described by the 3D Heisenberg model. A comparison with the critical behavior of the metal-rich halides Gd_2BrFe_2 and Gd_2IFe_2 supports our conclusion of a strong planar anisotropic exchange interaction induced by the 3*d* transition-metal atoms in these compounds.

ACKNOWLEDGMENTS

The authors are indebted to Dr. M. Seeger for fruitful discussions and to E. Brücher for performing the magnetic measurements.

* Present address: Max-Planck-Institut für Metallforschung, Institut für Physik, Postfach 800 665, D-70506 Stuttgart, Germany.

[1] R.K. Kremer, W. Bauhofer, Hj. Mattausch, W. Brill, and A. Simon, Solid State Commun. **73**, 281 (1990).

[2] C. Bauhofer, Hj. Mattausch, G.J. Miller, W. Bauhofer, R.K. Kremer, and A. Simon, J. Less-Common Met. **167**, 65 (1990).

[3] C. Michaelis, W. Bauhofer, H. Buckkremer-Hermanns, R.K. Kremer, and A. Simon, Z. Anorg. Chem. **618**, 98

(1992).
[4] R.K. Kremer, U. Beck, P. Fischer, and A. Simon, J. Magn. Magn. Mater. **140-144**, 1679 (1995).
[5] R.K. Kremer, J.K. Cockcroft, Hj. Mattausch, W. Schnelle, and A. Simon, J. Magn. Magn. Mater. **140-144**, 1187 (1995).
[6] M. Ruck and A. Simon, Z. Anorg. Chem. **619**, 327 (1993).
[7] R. Reisser, R.K. Kremer, and A. Simon, Physica B **204**, 265 (1995).
[8] S.N. Kaul, J. Magn. Magn. Mater. **53**, 5 (1985).
[9] R. Reisser, M. Seeger, M. Fähnle, and H. Kronmüller, J. Magn. Magn. Mater. **110**, 32 (1992).
[10] S.N. Kaul, Phys. Rev. B **38**, 9178 (1988).
[11] K. Kornik, H.P. Kunkel, R.M. Roshko, and G. Williams, Solid State Commun. **76**, 993 (1990).
[12] S.S.C. Burnett and S. Gartenhaus, Phys. Rev. B **43**, 591 (1991).
[13] S.N. Kaul and M. Sambasiva Rao, J. Phys. Condens. Matter **6**, 1 (1994).
[14] S.N. Kaul and Ch.V. Mohan, Phys. Rev B **50**, 6157 (1994).
[15] M. Seeger, S.N. Kaul, H. Kronmüller, and R. Reisser, Phys. Rev. B **51**, 12 585 (1995).
[16] F.J. Wegener, Phys. Rev. B **5**, 4529 (1972); M.E. Fisher, Rev. Mod. Phys. **46**, 597 (1974).
[17] A. Aharony and G. Ahlers, Phys. Rev. Lett. **44**, 782 (1980).
[18] Y. Yeshurun, M.B. Salamon, K.V. Rao, and H.S. Chen, Phys. Rev. B **24**, 1536 (1981).
[19] K. Westerholt, H. Bach, and R. Römer, J. Magn. Magn. Mater. **45**, 252 (1984).
[20] K.M. Lee, M.J. O'Shea, and D.J. Sellmyer, J. Appl. Phys. **61**, 3616 (1987).
[21] W.-U. Kellner, T. Albrecht, M. Fähnle, and H. Kronmüller, J. Magn. Magn. Mater. **62**, 169 (1986); W.-U. Kellner, M. Fähnle, H. Kronmüller, and S.N. Kaul, Phys. Status Solidi B **144**, 397 (1987).
[22] M. Haug, M. Fähnle, H. Kronmüller, and F. Haberey, J. Magn. Magn. Mater. **69**, 163 (1987); Phys. Status Solidi B **144**, 411 (1987).
[23] R. Reisser, M. Fähnle, and H. Kronmüller, J. Magn. Magn. Mater. **75**, 45 (1988).
[24] U. Güntzel and K. Westerholt, Phys. Rev. B **41**, 740 (1990).
[25] R. Reisser and H. Kronmüller, J. Magn. Magn. Mater. **98**, 273 (1991).
[26] R. Reisser, M. Seeger, and H. Kronmüller, J. Magn. Magn. Mater. **128**, 321 (1993).
[27] K.M. Lee and M.J. O'Shea, Phys. Rev. B **48**, 14 614 (1993).
[28] P. Gaunt, S.C. Ho, G. Williams, and R.W. Cochrane, Phys. Rev. B **23**, 251 (1981).
[29] M. Fähnle, W.-U. Kellner, and H. Kronmüller, Phys. Rev. B **35**, 3640 (1987).
[30] M. Seeger and H. Kronmüller, J. Magn. Magn. Mater. **78**, 393 (1989).
[31] R. Reisser and H. Kronmüller, J. Magn. Magn. Mater. **128**, 341 (1993).
[32] P.M. Gehring, M.B. Salamon, A. del Moral, and J.I. Arnaudas, Phys. Rev. B **41**, 9134 (1990).
[33] M.N. Deschizeaux and G. Develey, J. Phys. (Paris) **32**, 319 (1971).
[34] G.J.W. Geldart, P. Hargraves, N.M. Fujiki, and R.A. Dunlap, Phys. Rev. Lett. **62**, 2728 (1989).
[35] M. Seeger, Ph.D. thesis, University of Stuttgart, 1991.
[36] M. Fähnle and G. Herzer, J. Magn. Magn. Mater. **44**, 274 (1984).
[37] M. Fähnle, J. Magn. Magn. Mater. **65**, 1 (1987).
[38] M. Fähnle, J. Phys. C **16**, L819 (1983); Phys. Status Solidi B **130**, K113 (1985).
[39] M. Fähnle, J. Magn. Magn. Mater. **45**, 279 (1984).
[40] A. Aharony and E. Pytte, Phys. Rev. Lett. **45**, 1583 (1980).
[41] K. Ried, H. Gerth, D. Köhler, and H. Kronmüller, J. Magn. Magn. Mater. **109**, 275 (1992).
[42] K. Westerholt, J. Magn. Magn. Mater. **66**, 253 (1987).
[43] D. Köhler and H. Kronmüller, J. Magn. Magn. Mater. **92**, 344 (1991).
[44] M. Seeger, H. Kronmüller, and H.J. Blythe, J. Magn. Magn. Mater. **139**, 312 (1995).
[45] J.C. Le Guillou and J. Zinn-Justin, Phys. Rev. Lett. **39**, 95 (1977); J.C. Le Guillou and J. Zinn-Justin, Phys. Rev. B **21**, 3976 (1980); S.G. Gorishny, S.A. Larin, and F.V. Trachor, Phys. Rev. Lett. **101A**, 120 (1984); C. Bagnuls and C. Bervillier, Phys. Rev. B **32**, 7209 (1985).